

Image-based Visual Servoing for Nonholonomic Mobile Robots with Central Catadioptric Camera

Gian Luca Mariottini, Domenico Prattichizzo
Dipartimento di Ingegneria dell'Informazione
Università di Siena
Via Roma 56, 53100 Siena, Italy
Email: {gmariottini,prattichizzo}@dii.unisi.it

Giuseppe Oriolo
Dipartimento di Informatica e Sistemistica
Università di Roma "La Sapienza"
Via Eudossiana 18, 00184 Roma, Italy
Email: oriolo@dis.uniroma1.it

Abstract— We present an image-based visual servoing strategy for nonholonomic mobile robot equipped with a central catadioptric camera. This kind of vision sensor combines lens and mirrors to enlarge the field of view. The proposed approach, which exploits the epipolar geometry defined by the current and the desired camera views, does not need any knowledge of the 3-D scene geometry. The control scheme is divided in two steps. In the first one, the epipoles are used together with an approximate input-output linearizing feedback to align the robot with the goal. Feature points are then used in the second translation step to reach the desired configuration. Global asymptotic convergence is proven. Simulation and experimental results show the effectiveness of the proposed control scheme.

I. INTRODUCTION

This paper presents an image-based visual servoing (IBVS) strategy for driving a nonholonomic mobile robot to a desired configuration (*set-point*), which is specified only through a desired image previously acquired by an on-board omnidirectional camera.

In IBVS the control law is directly designed in the image domain, does not need any *a priori* knowledge of the 3-D structure of the observed scene and is robust with respect to model uncertainties and disturbances in both camera and robot models [11], [16]. Recently, there has been an increasing interest in the visual control of mobile robots subject to nonholonomic kinematic constraints. A first study of this kind can be found in [23] where the authors propose to use a pan-tilt camera, thus adding more degrees of freedom to the vision sensor, to control a mobile robot with the task function approach [6]. In [10], a piecewise-smooth visual servoing for mobile robots is presented. In both cases, however, a metrical knowledge of the observed scene is needed to guarantee the convergence to the desired configuration, thus limiting the applicability to a real context. However, the previous strategies do not consider the *visibility constraint*, i.e., the problem of keeping the relevant features in the camera field of view (FOV). In order to solve this problem some strategies have been investigated, e.g., based on zoom adjustment [15] or switching control [5]. All these strategies are specifically designed for robotic manipulators without nonholonomic constraints and cannot be easily generalized to take into account nonholonomy.

A completely different approach to the visibility constraint problem consists in using panoramic FOV provided by omnidirectional cameras, that naturally overcome the visibility constraint. We will refer to these sensors as *catadioptric cameras*, because they consist of a coupling between mirror (*catoptric* element) and conventional cameras with lenses (*dioptric* element).

Recently, applications of visual servoing using catadioptric cameras are growing in interest. A 3-D visual servoing with central catadioptric camera observing feature points has been studied in [1] and extended to the case of observed straight lines in [20]. In [4] is presented a visual servoing strategy for mobile robots equipped with central catadioptric cameras in which is necessary an estimation of the feature height to the plane of motion. All these approaches suffer from the same potential drawback, i.e., the control law is based on the inverse of the image Jacobian and can then become singular for certain configurations of the mobile robot or of the image feature position.

In order to overcome these problems, we propose an IBVS strategy for set-point global asymptotic stabilization of nonholonomic mobile robots to a target position. The robot is equipped with a central catadioptric camera. We only assume to know both the image acquired at the target position (*desired*) and the image at the current position (*current*) (see Fig. 10). The visual servoing uses the epipolar geometry existing between the current and the desired image [9]. This work is based on our previous contributions [17], [18] that are extended to central catadioptric cameras.

Our control algorithm consists of two sequential steps. The first compensates the orientation error so as to align the robot to its target configuration and is based on the use of an approximate input-output linearization with the system outputs depending on the epipole values. The second step leads the system to the target zeroing the translational displacement using the distance between corresponding image points. The resulting image-based visual servoing strategy guarantees global asymptotic convergence with exponential rate of the nonholonomic mobile robot to the desired configuration.

The main advantages of our approach are here outlined:

- Using the epipoles, we are able to avoid the problems arising from local minima and singularities that arise

when using the image Jacobian. Differently from [16], we do not estimate any relative camera displacement, but directly exploit the kinematics of epipoles in the image plane to design a global asymptotically stable control law.

- No metrical knowledge of the 3-D scene geometry is necessary, because epipoles can be computed from corresponding feature points in the current and desired view [9], [25].
- The visibility constraint is automatically satisfied by the adoption of a central catadioptric camera as a vision sensor.

The paper is organized as follows. Section II introduces the basics of central catadioptric cameras and their associated epipolar geometry. In Section III, the nonholonomic visual servoing problem is formulated and the 2-step control strategy is outlined. The first step is analyzed in Section IV, whenever Section V describes the feature-based control law which implements the second step. Simulation and experimental results are presented in Section VI and Section VII, to show the effectiveness of the proposed approach. In Section VIII, we provide some concluding remarks highlighting the main contributions of the paper.

II. BASIC EPIPOLAR GEOMETRY FOR CENTRAL CATADIOPTRIC CAMERAS

Several types of catadioptric cameras satisfy the *single viewpoint constraint*, i.e., the whole vision sensor only measures the light through a single point. This is necessary for the existence of epipolar geometry and for the generation of geometrically correct images [8]. In this case they are referred to as *central catadioptric cameras*, but we will hereafter refer to them only as catadioptric cameras, for short.

Consider the case in Fig. 1 in which a parabolic mirror is centered at the focus O and an orthographic camera is in front of it. Every scene point $P \in \mathbb{R}^3$ is projected onto the mirror surface at $X \in \mathbb{R}^3$ through O . The image point p (pixels) is obtained via orthographic projection of X . Note that a function $\eta : \mathbb{R}^3 \rightarrow \mathbb{R}^2$, dependent on known camera calibration parameters and mirror geometry, can be defined as a map from a mirror point X to its projection p onto the image plane, namely $\eta(X) = p$. More details can be found in [7].

Consider now two panoramic views as in Fig. 2, acquired by the same camera placed in O' and O , and referred to as *current*

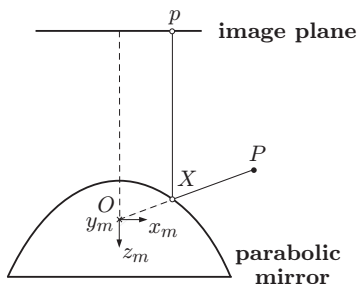


Fig. 1. Imaging model of a catadioptric camera (e.g. orthographic camera coupled with parabolic mirror).

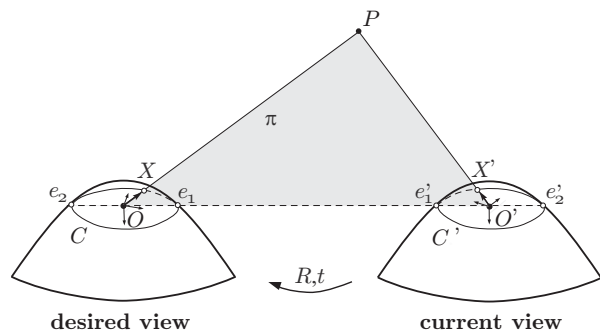


Fig. 2. Basic epipolar geometry setup for catadioptric cameras. Every epipolar plane contains the baseline and intersects the mirror at the epipolar conic.

and *desired* views, respectively. Without loss of generality, we choose the world reference frame coincident with the one at the desired view. Camera parameters are supposed to be known and consequently the epipolar geometry can be directly expressed onto the mirror surface if not otherwise specified. The segment $\overline{OO'}$, called *baseline*, intersects the two mirror surfaces at the *epipoles*, namely e_1 and e_2 for the current view, and e'_1 and e'_2 for the desired view. The *epipolar plane* π intersects each mirror at the *epipolar conics* C and C' . Each epipolar conic passes through the epipoles.

Given a pair of views of a set of scene points P_i ($i = 1, \dots, n$) there exists a matrix $E \in \mathbb{R}^{3 \times 3}$, called the *essential matrix* [9], such that

$$X_i^T E X'_i = 0 \quad (1)$$

for all corresponding mirror points X_i and X'_i (i.e., images of the same point in the two views), obtained as a back-projection of the corresponding image points p_i and p'_i , by means of the inverse of η . In general, the essential matrix is of rank 2 and is defined up to an arbitrary scale. Given at least 5 generic correspondences E can be computed up to a scale factor, without any knowledge of the 3-D structure of the observed scene [9]. In presence of image noise, E can be robustly estimated also by means of well known algorithms, e.g., [14], [26]. We are here particularly interested in retrieving the epipole direction in both views. We will henceforth assume to be able to have the right guess of where is the epipole directly pointing toward the other view (i.e., e_1 and e'_1 in Fig. 2). The current and desired epipoles can then be retrieved from the left and right null-spaces of E [9].

Remark 1: Suppose given two views p and p' , the current and the desired, of the same 3-D scene point P , respectively. Suppose, moreover, that only a translation $t = [x \ y \ z]^T$ occurs between their coordinate frames (i.e., $R = I$). It is an easy matter to see that, for any translational motion of the camera along t , the epipolar conic C' associated with (p, p') does not vary and p' will lie on it. In fact, the normal vector of the epipolar plane does not vary for any scaling $\lambda \in \mathbb{R} - \{0\}$, thus keeping constant the shape of C' .

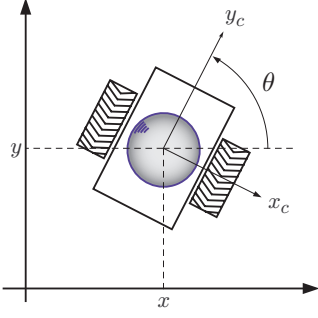


Fig. 3. A mobile robot with unicycle kinematics carrying a catadioptric camera.

III. THE NONHOLONOMIC VISUAL SERVOING PROBLEM

The objective of this work is to present an image-based visual servoing strategy that drives a nonholonomic robot toward a desired configuration. The nonholonomic mobile robot considered in this paper is a unicycle moving on a plane (see Fig. 3). Its configuration vector is defined by $q = [x y \theta]^T$, where x, y are the Cartesian coordinates (in meters) of the center of the robot in a reference frame $\{O, x, y\}$, being θ (in radians) the orientation with respect to the x axis (see Fig. 3). The nonholonomic kinematic model is

$$\begin{aligned}\dot{x} &= u_1 \cos \theta \\ \dot{y} &= u_1 \sin \theta \\ \dot{\theta} &= u_2\end{aligned}\quad (2)$$

where u_1 and u_2 are respectively the translational and the angular velocity. Without loss of generality, we suppose that the desired configuration is $q_d = [0 0 \pi/2]^T$, which corresponds to the robot being centered at the origin and aligned with the positive y axis. The catadioptric camera is fixed to the robot body in such a way that the mirror focus O' is in $[x y]^T$.

In the spirit of the visual servoing approach, it is henceforth assumed that the desired camera view (i.e., the view acquired in q_d) has been gathered in advance and that the epipoles are estimated in real-time according to the techniques described in Sect. II. Let us consider the situation in Fig. 4. Let y_1 and

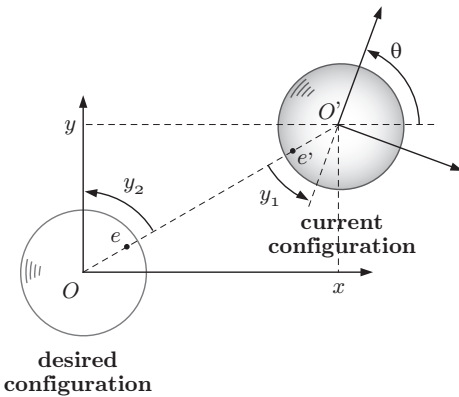


Fig. 4. The planar geometric setup used to define the kinematics of outputs, written as a function of the epipoles.

y_2 be the two outputs of the system that can be written as a function of the epipoles $e = [e_x e_y e_z]^T$ and $e' = [e'_x e'_y e'_z]^T$, expressed in the mirror frame, as follows:

$$y_1 = -\frac{\pi}{2} - \text{ATAN2}\{e'_y, e'_x\} \quad (3)$$

$$y_2 = \frac{\pi}{2} - \text{ATAN2}\{e_y, e_x\}. \quad (4)$$

The proposed image-based visual servoing scheme drives the nonholonomic mobile robot to the desired configuration q_d in two steps (see Fig. 5):

- 1) From the initial configuration q_0 , apply a control law that brings y_1 and y_2 to zero. As shown in the next section, such a control may be computed through input-output feedback linearization. At the end of this step the camera-robot is in the intermediate configuration q_i , aligned with the desired one (see Fig. 5, left).
- 2) From the intermediate configuration q_i apply another image-based control producing a translation to q_d (see Fig. 5, right). Clearly, y_1 and y_2 are identically zero in this phase and cannot be used. However, as will be shown next, this step can be realized on the basis of corresponding points in the images.

Roughly speaking, the first step is aimed at zeroing the orientation error (and placing the robot along the y -axis) while the second step compensates the translation error.

IV. FIRST STEP: ZEROING THE EPIPOLES

We here design a visual feedback for the mobile robot in order to drive both outputs to zero and realize the first step of our visual control strategy. To this end, after deriving the epipole kinematics, we adopt an approximate input-output linearization approach. For our visual servoing purposes it is paramount to remark that these outputs can be written as a function of the epipoles e and e' , as in (3) and (4).

From Fig. 4 it may be also seen that

$$y_1 = y_2 + \theta - \frac{\pi}{2}. \quad (5)$$

Differentiating (5) we have:

$$\dot{y}_1 = u_2 + \dot{y}_2. \quad (6)$$

From (4), the first derivative of y_2 is

$$\dot{y}_2 = \dot{e}_x \frac{e_y}{e_x^2 + e_y^2} - \dot{e}_y \frac{e_x}{e_x^2 + e_y^2}. \quad (7)$$

From Fig. 4, let $d \triangleq (x^2 + y^2)^{1/2}$, being $e_x = \lambda x$ and $e_y = \lambda y$ for an unknown $\lambda \in \mathbb{R}$, and $x = d \sin y_2$ and $y = d \cos y_2$. Then from (7) it yields

$$\dot{y}_2 = \frac{u_1}{d} \cos(\theta + y_2). \quad (8)$$

Now, substituting (5) in (8) we get:

$$\dot{y}_1 = u_2 - u_1 \frac{\sin y_1}{d} \quad (9)$$

$$\dot{y}_2 = -u_1 \frac{\sin y_1}{d} \quad (10)$$

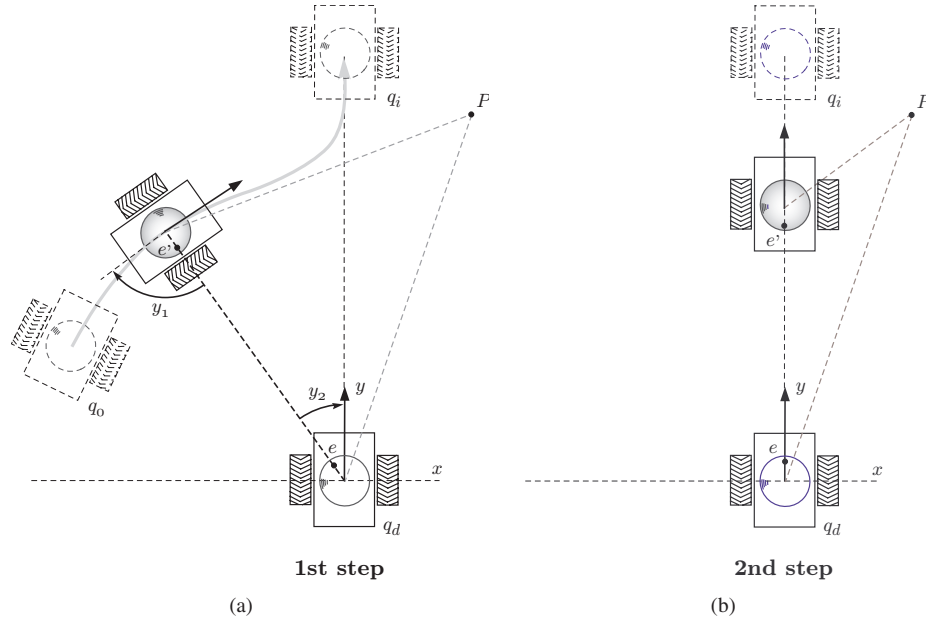


Fig. 5. The two steps of the proposed visual servoing strategy. (a) The nonholonomic robot is first driven to the y axis by zeroing both outputs y_1 and y_2 . (b) A feature-based controller is then used to recover the translation error.

The standard procedure to compute an input-output linearizing control law is to differentiate the output functions and invert, if possible, the resulting map (see [12]). From the epipole differential kinematics (9-10), the relationship between the control inputs and the output time derivatives is expressed as

$$\begin{bmatrix} \dot{y}_1 \\ \dot{y}_2 \end{bmatrix} = E \begin{bmatrix} u_1 \\ u_2 \end{bmatrix} \quad \text{with} \quad E = \begin{bmatrix} -\frac{\sin y_1}{d} & 1 \\ -\frac{\sin y_1}{d} & 0 \end{bmatrix}.$$

Here, we are faced with a major difficulty, i.e., the inverse of the decoupling matrix E cannot be computed because the parameter d (the distance between the current and the desired robot position) is unknown in the purely image-based control framework we are dealing with. Although this prevents from performing an exact input-output, an approximate input-output linearization strategy can be pursued by setting

$$\begin{bmatrix} u_1 \\ u_2 \end{bmatrix} = \hat{E}^{-1} \begin{bmatrix} \nu_1 \\ \nu_2 \end{bmatrix} \quad (11)$$

with

$$\hat{E}^{-1} = \begin{bmatrix} 0 & -\frac{\hat{d}}{\sin y_1} \\ 1 & -1 \end{bmatrix}.$$

in which an estimate \hat{d} of d is used and the resulting output derivatives are

$$\begin{bmatrix} \dot{y}_1 \\ \dot{y}_2 \end{bmatrix} = E \hat{E}^{-1} \begin{bmatrix} \nu_1 \\ \nu_2 \end{bmatrix} = \begin{bmatrix} 1 & \frac{\hat{d}}{d} - 1 \\ 0 & \frac{\hat{d}}{d} \end{bmatrix} \begin{bmatrix} \nu_1 \\ \nu_2 \end{bmatrix}$$

Proposition 1: Let

$$\begin{bmatrix} \nu_1 \\ \nu_2 \end{bmatrix} = \begin{bmatrix} -k_1 y_1 \\ -k_2 y_2^{\beta/\gamma} \end{bmatrix} \quad (12)$$

where $k_1 > 0$, $k_2 > 0$ and β, γ are positive odd integers, with $\beta < \gamma$. Also, update the distance estimate \hat{d} according to

$$\dot{\hat{d}} = \hat{d} k_2 \frac{y_2^{\beta/\gamma}}{\tan y_1} \quad (13)$$

initialized at $\hat{d}_0 > d_0$, being d_0 the distance from the initial to the desired robot configurations. Then, for sufficiently small k_2 , the approximately linearizing control (11) drives both output coordinates y_1 and y_2 to zero for any initial condition with exponential convergence rate.

Proof. First of all note that the closed-loop equations under the proposed control law are

$$\dot{y}_1 = -k_1 y_1 - \left(\frac{\hat{d}}{d} - 1 \right) k_2 y_2^{\beta/\gamma} \quad (14)$$

$$\dot{y}_2 = -\frac{\hat{d}}{d} k_2 y_2^{\beta/\gamma} \quad (15)$$

while the explicit expression for the control inputs in (11) is:

$$u_1 = \hat{d} k_2 \frac{y_2^{\beta/\gamma}}{\sin y_1} \quad (16)$$

$$u_2 = -k_1 y_1 + k_2 y_2^{\beta/\gamma}. \quad (17)$$

The distance d evolves according to $\dot{d} = \frac{x\dot{x} + y\dot{y}}{d}$ and using (2) and being $x = d \sin y_2$ and $y = d \cos y_2$ we get

$$\dot{d} = u_1 \cos y_1 = \hat{d} k_2 \frac{y_2^{\beta/\gamma}}{\tan y_1}. \quad (18)$$

Comparing (18) with (13), it is clear that d and \hat{d} obey to the same differential equation. Hence,

$$\frac{\dot{\hat{d}}}{\hat{d}} = \frac{\dot{d}_0 + \int_0^t \dot{\hat{d}} dt}{d_0 + \int_0^t \dot{\hat{d}} dt} = 1 + \frac{\hat{d}_0 - d_0}{d} > 1$$

under the assumption $\hat{d}_0 > d_0$. As a consequence, the coefficient of $y_2^{\beta/\gamma}$ in (15) is negative and bounded below in modulus. This means that 0 is a terminal attractor [27] for y_2 , which will converge to zero at a finite time instant \bar{t} . Then from \bar{t} on, the differential equation (14) governing y_1 reduces to $\dot{y}_1 = -k_1 y_1$, so that y_1 will converge to zero with exponential rate k_1 . As a consequence, it can be seen from (18) that due to the zeroing of y_2 at \bar{t} , the robot converges at a finite distance d after \bar{t} , as shown by (18). In conclusion, note also that (16) is never singular because u_1 becomes zero after \bar{t} .

It remains to be shown that the control input in (16-17) is not singular. In fact, the linear velocity in (17) has a potential singularity when $y_1 = 0$. This is not a problem for $t \geq \bar{t}$, for which u_1 is identically zero, being $y_2 = 0$. Before \bar{t} , the dynamics of y_1 in (14) include a ‘perturbation’ term whose effect can be arbitrarily bounded by bounding k_2 . Hence, for sufficiently small k_2 , the output y_2 can not cross zero during the transient. ■

The following remarks are in order at this point.

- The above control law is purely image-based because it only relies on the measured epipoles. No knowledge of the robot configuration or any other odometric data is needed.
- The particular form of the exponent of y_2 in the control law (12) is essential in guaranteeing its convergency to zero in *finite time*, and then that the proposed control law is never singular. This kind of control law is also known as a *terminal sliding mode*.
- According to the above Prop. 1, it is necessary to initialize \hat{d} at an initial value $\hat{d}_0 > d_0$. To this end one may use an upper bound on d_0 derived from the knowledge of the environment where the robot moves.
- If y_1 is zero at the initial instant, then \hat{E}^{-1} is undefined in (11). Then, it is necessary to perform a preliminary maneuver (e.g., a fixed rotation) before applying the proposed controller, in order to attain a nonzero y_1 .
- The *zero dynamics* (i.e., the residual dynamics when the outputs are identically zero [12]) associated with our approximate input-output linearization controller is obtained from (18) as $\dot{d} = 0$. That is, the robot will converge to some point of the y axis at a *finite* distance d from its desired position, consistently with the above proof.

V. SECOND STEP: FEATURES MATCHING

At the end of the first step, both the outputs y_1 and y_2 are zero and the intermediate robot configuration q_i is aligned with the desired configuration (see Fig. 5, right). We now present the feature-based control law that realizes the second step of our visual servoing strategy, i.e., moving the robot from q_i to q_d so as to recover the translation error. As the epipole-based controller of the previous section, also the second step controller works directly in the camera image plane.

The basic idea consists in translating the robot until each feature p'_i ($i = 1, \dots, n$) in the current image plane matches the corresponding one p_i in the desired image plane. A similar

approach has been proposed in [2], [24] for pinhole cameras. As shown in Sect. II, if the relative rotation is compensated, then during a translational motion to the target position along the baseline, all feature points p'_i converge to p_i and are constrained also to lie on the corresponding epipolar conic C'_i . Then the feature distance between corresponding points, chosen as the arc-length $s'_i(t)$ between p_i and p'_i onto C'_i , will be zero when $p'_i = p_i$, i.e., when the robot reaches the final configuration q_d . In principle, only one feature is needed to implement this idea, and therefore we will present the controller with reference to the case $n = 1$. The proposed method can be easily extended to include a larger number of features, a convenient choice in the case of noisy images.

Proposition 2: Let the robot velocities during the second step be defined as

$$u_1 = -k_t s'_i(t) e_y \quad (19)$$

$$u_2 = 0 \quad (20)$$

where $k_t > 0$. Then the robot configuration converges exponentially from the intermediate configuration q_i to the origin.

Proof. We here consider that the rotation disparity with respect to the desired robot-camera configuration has been fully compensated during the first step, i.e., $\theta_i = \pi/2$ that corresponds to $e_x = e'_x = 0$.

Consider the positive definite Lyapunov function $V = (x^2 + y^2)/2$. Note that $e_x = \lambda x$ and $e_y = \lambda y$ for an unknown positive λ . Being $e_x = 0$ (i.e., $\theta = \pi/2$), then the time derivative of V yields to $\dot{V} = x\dot{x} + y\dot{y} = \frac{u_1}{\lambda} e_y$. Substituting (19) in it, we obtain $\dot{V} = -k_t s'_i e_y^2$ that is always definite negative, being $s'_i(t) > 0$. Note that $s'_i(t)$ acts as a stop condition, because it clearly zeroes when $p'_i = p_i$. ■

VI. SIMULATION RESULTS

The simulation results have been performed using Matlab-Simulink and the Epipolar Geometry Toolbox [19]. It is assumed that five pairs of corresponding feature points are identified in the desired and current image. The camera calibration parameters [9] are $f_x = f_y = 10^2$ mm. and $u_0 = 320$ pixels and $v_0 = 240$ pixels. The unicycle robot moves under the action of the proposed two-step visual strategy from its

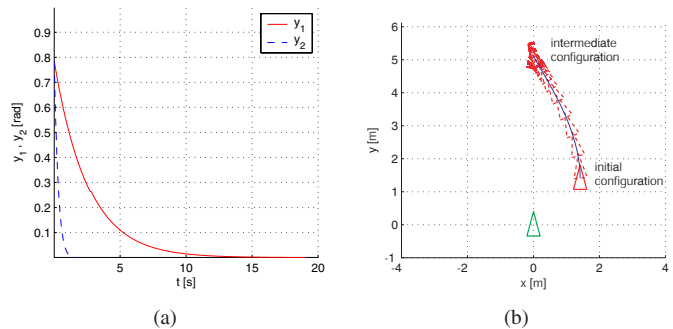


Fig. 6. Nominal case. First Step. (a) Outputs behavior. Note how the second output coordinate y_2 reaches zero in finite time; (b) Robot trajectory.

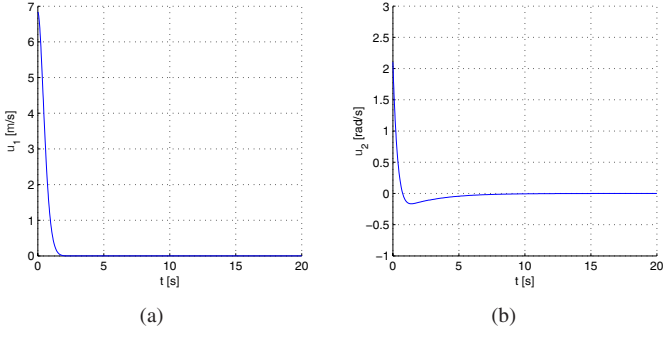


Fig. 7. Nominal case. First Step. (a) Linear velocity and (b) angular velocity of the mobile robot. Note how the linear velocity goes to zero with y_2 .

initial configuration $q_0 = [\sqrt{2} \sqrt{2} \pi/2]^T$ to the desired one $q_d = [0 0 \pi/2]^T$.

First the control law in (11) is applied with $k_1 = 0.4$, $k_2 = 3$ and $\beta/\gamma = 17/19$. The initial estimate of the robot distance has been set to $\hat{d}_0 = 4$ m. As shown in Fig. 6(a), both the output coordinates y_1 and y_2 are driven to zero and, as expected, the first one is zeroed in finite time $t = 2$ sec. The robot trajectory for the first step is reported in Fig. 6(b) while the resulting control inputs are shown in Fig. 7(a)-(b). To guarantee a finite time duration of the first step, a tolerance of 10^{-9} m. has been used for y_1 (recall that convergence is exponential).

The second step is then executed under the action of the control law in (11), with $k_t = 10^4$. The exponential decrease of the distance $s(t)$ between the current and the desired feature points along the conic is shown in Fig. 8(a). The robot trajectory in the second step is reported in Fig. 8(b).

VII. EXPERIMENTAL RESULTS

In order to validate the here proposed visual servoing strategy we present some experimental results realized in our labs. The vision sensor is a folded catadioptric mirror [3] by Remote Reality screwed on a CCD camera by Lumenera Inc. Such a camera can be modeled by an orthographic camera looking at a parabolic mirror [21] modeled by the equation $z_m + \frac{a}{2} = \frac{x_m^2 + y_m^2}{2a}$ where $a = 33.4$ mm. The mobile robot is

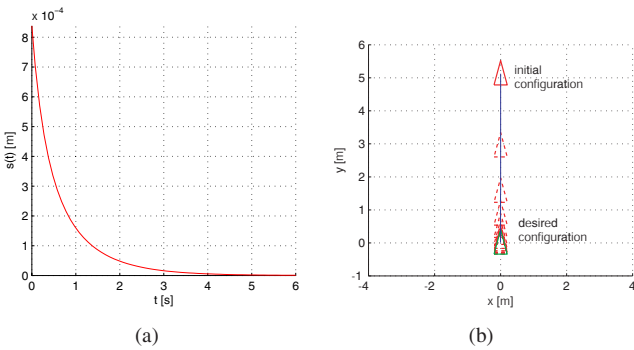


Fig. 8. Nominal case. Second Step. (a) Exponential decrease of the distance s between the current and the desired features in the image planes; (b) Robot trajectory.

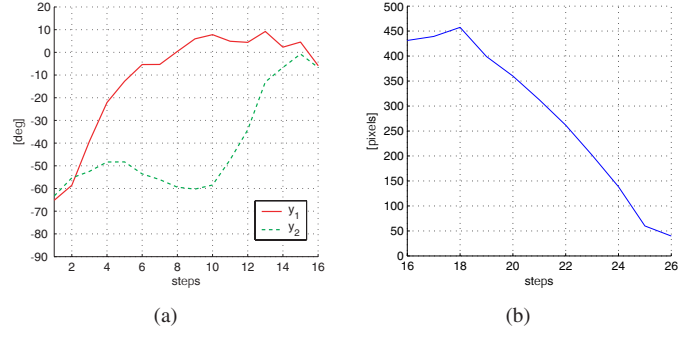


Fig. 9. Experimental results. (a) Outputs variables y_1 and y_2 are controlled to zero by the image-based control law; (b) Distance (in pixels) from current to target image feature points measured on the epipolar conic.

an Pioneer 2X-DE by ActivMedia, connected to a notebook endowed with a 2 GHz Pentium 4 processor and with 640 MB of RAM. Orthographic camera parameters are $f_x = 13$ mm., $f_y = 14$ mm., $u_0 = 616.3$ and $v_0 = 628.2$ pixels. A set of $n = 9$ corresponding feature points has been tracked and used for epipolar geometry estimation using the robust *M-estimator* proposed in [26]. In order to obtain a better epipolar geometry estimation, we normalized all feature points as suggested in [3].

Fig. 9(a) shows the outputs that are driven to zero during the first step. Note that, due to image noise affecting the epipolar geometry estimation, perfect convergence of outputs to zero can not be achieved. However, as expected, y_2 is the first output to reach zero, followed by y_1 . After both outputs are below (in modulus) a specified threshold ($\tau_v = 7$ deg.), then the second step starts and the mean distance of $s_i(t)$ between corresponding points is used to control the translation (Fig. 9(b)). It can be seen that it rapidly decreases to zero, but due to image noise, to the non perfect alignment

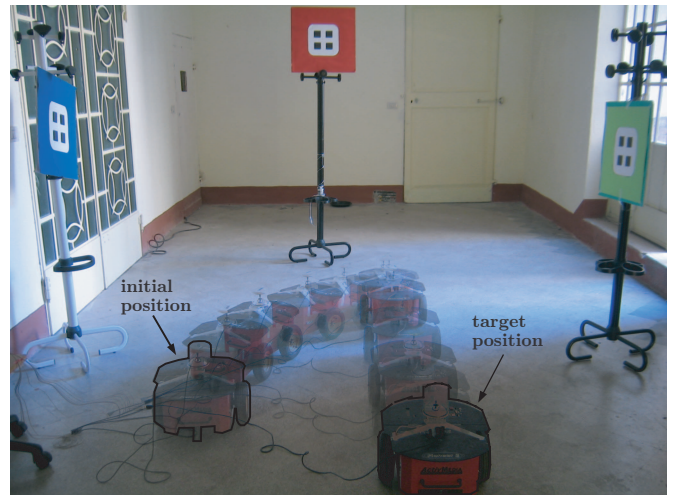


Fig. 10. Experimental results. The Pioneer 2X-DE robot is equipped with a panoramic camera and correctly moves toward the target position using only the visual information provided by the current and the desired panoramic images.

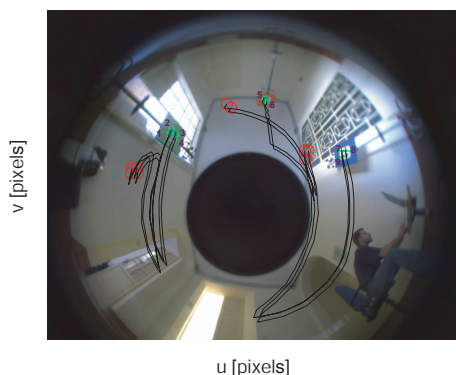


Fig. 11. Experimental results. Feature motion on the image plane superimposed to the desired image, starting from the initial features (circle) to the desired ones (cross).

after the first step and to model uncertainties, we obtained a final distance of about 5 pixels for each of the 9 feature pairs. This corresponds in a robot displacement of about 2 cm with respect to the target position. However it is our plan to improve performances and increase robustness by setting the proposed two-step controller in an iterative framework as proposed in [13], [22] for nonholonomic robots. The robot motion under the action of the proposed control law, from the starting position to the target one, is reported in Fig. 10. The whole feature motion in the image plane is shown in Fig. 11 and superimposed to the desired image, thus showing the convergence to the target image features.

VIII. CONCLUSIONS

A novel image-based visual servoing strategy has been presented for nonholonomic mobile robots. The control scheme, which is divided in two independent and sequential steps, drives the robot to a desired configuration specified through a target view, previously acquired by the on-board central catadioptric camera. A key point is the use of multiple-view epipolar geometry during the first step in order to compensate the rotational error and align the current view to the desired one. In particular, an approximate input-output linearizing feedback law is used to cope with the nonholonomic kinematics of the camera-robot system. Simulations and experimental results have been performed in order to validate the proposed visual servoing algorithm.

REFERENCES

- [1] J.P. Barreto, F. Martin, and R. Horaud. Visual servoing/tracking using central catadioptric images. In *8th International Symposium on Experimental Robotics*, pages 863–869, 2002.
- [2] R. Basri, E. Rivlin, and I. Shimshoni. Visual homing: Surfing on the epipoles. *International Journal of Computer Vision*, 33(2):117–137, 1999.
- [3] R. Benosman and S.B. Kang. *Panoramic Vision: Sensors, Theory and Applications*. Springer Verlag, New York, 2001.
- [4] D. Burschka and G. Hager. Vision-based control of mobile robots. In *2001 IEEE International Conference on Robotics and Automation*, pages 1707–1713, 2001.

- [5] G. Chesì, K. Hashimoto, D. Prattichizzo, and A. Vicino. Keeping features in the field of view in eye-in-hand visual servoing: a switching approach. *IEEE Transactions on Robotics*, 20(5):908–914, 2004.
- [6] B. Espiau, F. Chaumette, and P. Rives. A new approach to visual servoing in robotics. *IEEE Transactions on Robotics and Automation*, 8(3):313–326, 1992.
- [7] C. Geyer and K. Daniilidis. A unifying theory for central panoramic systems. In *Proc. of Sixth European Conference on Computer Vision*, pages 445–462, 2000. Dublin, Ireland.
- [8] C. Geyer and K. Daniilidis. Mirrors in motion: Epipolar geometry and motion estimation. In *9th IEEE International Conference on Computer Vision*, volume 2, pages 766–773, 2003.
- [9] R. Hartley and A. Zisserman. *Multiple View Geometry in Computer Vision*. Cambridge University Press, 2000.
- [10] K. Hashimoto and T. Noritsugu. Visual servoing of nonholonomic cart. In *1997 IEEE International Conference on Robotics and Automation*, pages 1719–1724, 1997.
- [11] S.A. Hutchinson, G.D. Hager, and P.I. Corke. A tutorial on visual servo control. *IEEE Transactions on Robotics and Automation*, 12(5):651–670, 1996.
- [12] A. Isidori. *Nonlinear Control Systems*. Springer, 1995.
- [13] P. Lucibello and G. Oriolo. Robust stabilization via iterative state steering with an application to chained-form systems. *Automatica*, 37:71–79, 2001.
- [14] Q.T. Luong and O.D. Faugeras. The fundamental matrix: theory, algorithms and stability analysis. *International Journal of Computer Vision*, 17(1):43–76, 1996.
- [15] E. Malis and S. Benhimane. Vision-based control with respect to planar and non-planar objects using a zooming camera. In *2004 IEEE International Conference on Advanced Robotics*, pages 863–869, 2004.
- [16] E. Malis, F. Chaumette, and S. Boudet. 2-1/2-D visual servoing. *IEEE Transactions on Robotics and Automation*, 15(2):238–250, 1999.
- [17] G.L. Mariottini, G. Oriolo, and D. Prattichizzo. Epipole-based visual servoing for nonholonomic mobile robots. In *2004 IEEE International Conference on Robotics and Automation*, volume 1, pages 497 – 503, 2004.
- [18] G.L. Mariottini, G. Oriolo, and D. Prattichizzo. Image-based visual servoing for nonholonomic mobile robots using epipolar geometry. *IEEE Transactions on Robotics*, 2005. Submitted.
- [19] G.L. Mariottini and D. Prattichizzo. The Epipolar Geometry Toolbox: multiple view geometry and visual servoing for MATLAB. *IEEE Robotics and Automation Magazine*, 2005. to appear.
- [20] Y. Mezouar, H. Haj Abdelkader, P. Martinet, and F. Chaumette. Central catadioptric visual servoing from 3d straight lines. In *2004 IEEE/RSJ International Conference on Intelligent Robots and Systems*, volume 1, pages 343–349, 2004.
- [21] S.K. Nayar. Catadioptric omnidirectional camera. In *Proc. of International Conference on Computer Vision and Pattern Recognition*, pages 482–488, 1997.
- [22] G. Oriolo and M. Vendittelli. A framework for the stabilization of general nonholonomic systems with an application to the plate-ball mechanism. *IEEE Transactions on Robotics*, 21(2):162–175, 2005.
- [23] R. Pissard-Gibollet and P. Rives. Applying visual servoing techniques to control a mobile hand-eye system. In *1995 IEEE International Conference on Robotics and Automation*, pages 166–171, 1995.
- [24] T. Sato and J. Sato. Visual servoing from uncalibrated cameras for uncalibrated robots. *Systems and Computers in Japan*, 31(14):11–19, 2000.
- [25] T. Svoboda and T. Pajdla. Epipolar geometry for central catadioptric cameras. *International Journal of Computer Vision*, 49(1):23–37, 2002.
- [26] P.H.S. Torr and D.W. Murray. The development and comparison of robust methods for estimating the fundamental matrix. *International Journal of Computer Vision*, 24(3):271–300, 1997.
- [27] M. Zak. Terminal attractors in neural networks. *Neural Networks*, 2:259–274, 1989.